TPR-Mediated Self-Association of Plant SGT1[†]

Afua Nyarko,[‡] Khédidja Mosbahi,[‡] Arthur J. Rowe,[§] Andrew Leech,[‡] Marta Boter,[∥] Ken Shirasu,[∥,⊥] and Colin Kleanthous*,[‡]

Department of Biology, University of York, PO Box 373, York, YO10 5YW, U.K., NCMH Business Center, School of Biosciences, University of Nottingham, Sutton Bonington, Leicestershire, LE12 5RD, U.K., and The Sainsbury Laboratory, John Innes Center, Colney Lane, Norwich, NR4 7UH, U.K.

Received April 18, 2007; Revised Manuscript Received August 2, 2007

ABSTRACT: The tetratricopeptide repeat (TPR) domain mediates inter-protein associations in a number of systems. The domain is also thought to mediate oligomerization of some proteins, but this has remained controversial, with conflicting data appearing in the literature. By way of investigating such TPR-mediated self-associations we used a variety of biophysical techniques to characterize purified recombinant Sgt1, a TPR-containing protein found in all eukaryotes that is involved in a broad range of biological processes, including kinetochore assembly in humans and yeast and disease resistance in plants. We show that recombinant Sgt1 from *Arabidopsis*, barley, and yeast self-associates *in vitro* while recombinant human Sgt1 does not. Further experiments on barley Sgt1 demonstrate unambiguously a TPR-mediated dimerization, which is concentration- and ionic-strength-dependent and results in a global increase in helical structure and stability of the protein. Dimerization is also redox sensitive, being completely abolished by the formation of an intramolecular disulfide bond where the contributing cysteines are conserved in plant Sgt1s. The dimer interface was mapped through cross-linking and mass spectrometry to the C-terminal region of the TPR domain. Our study, which provides the first biophysical characterization of plant Sgt1, highlights how TPR domains can mediate self-association in solution and that sequence variation in the regions involved in oligomerization affects the propensity of TPR-containing proteins to dimerize.

The tetratricopeptide repeat (TPR[1]) is a common intracellular motif that mediates protein−protein interactions in organisms ranging from bacteria to humans (reviewed in ref *1*). It was first identified in several proteins required for mitosis and RNA synthesis in *Saccharomycese cerevisiae (2*), but has since been shown to be more widespread and is found in various subcellular locations including the cytoplasm, nucleus, and mitochondria. The TPR motif is a degenerate 34-amino acid sequence usually occurring in tandem repeats of 3−16, with individual motifs or blocks of motif dispersed throughout the protein (*3*). A common feature of the motif is a consensus sequence defined by a pattern of small and large hydrophobic amino acids with the small amino acids usually found in positions 8, 20, and 27 (*1*). The rationale for the consensus sequence became clear with the high-resolution structure of the TPR domain of protein phosphatase 5 (PP5). PP5 has three TPR motifs each composed of a pair of antiparallel α-helices, which adopt a helix−turn−helix arrangement. Helix packing results in residues 8 and 20 being at positions of closest contact between the helices, while residue 27 is located at the interface of three helices, hence the need for the small amino acids at these sites. The overall packing of the helices within and between individual TPR motifs generates a right-handed superhelical conformation that creates an amphipathic channel, which serves as a binding site for interacting proteins (*4*).

The TPR motif is found in proteins with diverse functions (http://www.ebi.ac.uk/integr8) (*5*). Included in this list is human PP5 (*6*), the mouse acetylcholine receptor-associated protein, rapsyn (*7*), and the *Saccharomyces cerevisiae* cell cycle control proteins, Cdc16, Cdc23, and Cdc27 (*8*). The interactions of these proteins may involve direct associations with other TPR proteins, as has been observed between Cdc16, Cdc27, and PP5 (*9*, *10*) or with non-TPR proteins, observed between Hop/Sti1 and Hsp70/Hsp90 (*11*). Intermolecular TPR interactions resulting in self-associations have also been noted, although in a number of cases the relevance of such self-associations to the solution properties of TPR-containing proteins remains unclear (*1*, *12*, *13*). A case in point is the TPR-mediated self-association of PP5. The crystal structure of the isolated TPR domain showed an interaction between the C-terminal helix and the concave surface of a neighboring molecule resulted in the formation of dimers. This dimerization was attributed to a "crystallographic artifact" since the solution properties monitored

[†] This work is supported by the Biotechnology and Biological Sciences Research Council (BBSRC) of the U.K.

* Corresponding author. Tel: +44 (0) 1904 328820. Fax: +44 (0) 1904 328825. E-mail: ck11@york.ac.uk.

[‡] University of York.

[§] University of Nottingham.

[∥] The Sainsbury Laboratory, John Innes Center.

[⊥] Current address: RIKEN Plant Science Center, 1-7-22 Suehiro, Tsurumi, Yokohama 230-0045, Japan.

[1] Abbreviations: Sgt 1, suppressor of G2 allele of Skp1; His-AtSgt1b, His-HvSgt1, His-HsSgt1, His-ScSgt1, constructs of *Arabidopsis thaliana*, *Hordeum vulgare*, *Homo sapiens*, and *Saccharomyces cerevisiae* Sgt1, respectively, that include an N-terminal hexa-histidine tag; CD, circular dichroism; DSS, disuccinimidyl suberate; TCEP, Tris (2-carboxyethyl) phosphine hydrochloride; TPR, tetratricopeptide repeat; DTT, dithiothreitol; PBS, phosphate buffered saline.

10.1021/bi700735t CCC: $37.00
Published on Web 09/18/2007

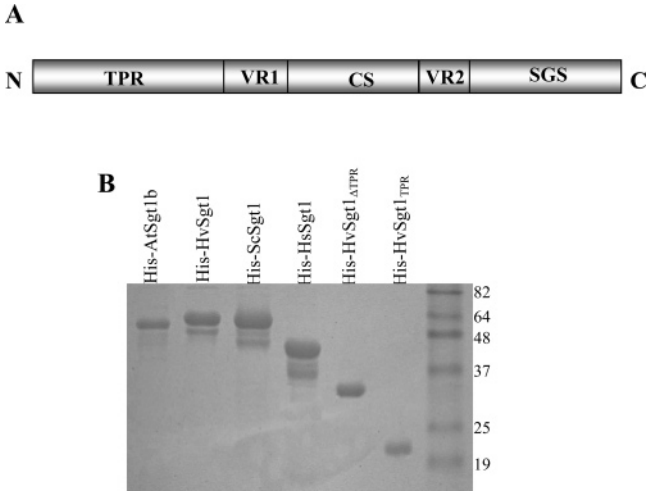

FIGURE 1: Domain organization of Sgt1 and purity of constructs used in this work. (A) Sgt1 is made up of an N-terminal tetratricopeptide repeat (TPR) domain, a middle CHORD and SGT1 (CS) domain sandwiched between two variable regions, VR1 and VR2, and a C-terminal "SGT1 specific" (SGS) domain. (B) A 15% SDS−polyacrylamide gel showing the purity of the histidine-tagged proteins used in this work: *Arabidopsis thaliana* Sgt1b (His-AtSgt1b), barley (His-HvSgt1), baker's yeast (His-ScSgt1), and human (HsSgt1). His-HvSgt1$_{TPR}$ and His-HvSgt1$_{\Delta TPR}$ are constructs of barley Sgt1 with or without the TPR domain, respectively. Faster migrating bands observed for His-HvSgt1, His-ScSgt1, and His-HsSgt1 are degradation products that copurify with the full length proteins.

by analytical size-exclusion chromatography experiments did not detect the presence of species other than the monomer (*4*, *12*). Similarly, intermolecular interactions have been observed for both monoclinic and tetragonal crystal forms of Cyclophilin 40, but whether these reflect the solution properties is uncertain (*14*). Given the importance of TPR domains in interprotein associations, the possibility that such domains could engage in self-associations in solution would have important regulatory consequences. We therefore addressed this question in Sgt1, a conserved and essential eukaryotic protein.

Sgt1 is involved in a broad range of functions that are usually elicited through interactions with multi-protein complexes. In plants it is a key regulator of race-specific disease resistance with additional roles in the auxin response pathway and protein degradation via the 26 S proteasome (*15*−*19*). Yeast Sgt1 associates with the SCF ubiquitin ligase complex and is required for the assembly of the kinetochore (*20*). Human Sgt1 is also required for the assembly of the kinetochore (*21*) and has recently been shown to positively regulate Nod1 activation, suggesting a role of the protein in innate immunity (*22*). The three-dimensional structure of Sgt1 is not known, but primary sequence analyses across species has identified distinct protein−protein interaction motifs, including an N-terminal TPR domain, a central "CHORD and SGT1" or CS domain, and a C-terminal "SGT1 specific" or SGS domain (*15*, *23*, *24*) (Figure 1). The associations of each of these domains have been well documented. For example, the TPR domain of yeast Sgt1 binds Skp1, a protein of the SCF ubiquitin ligase complex (*20*), the CS domain of human, plant, and yeast Sgt1 binds Hsp90 (*25*−*27*), and the SGS domain of human Sgt1 associates with rabbit calcyclin (S100A6) (*28*).

We report a series of biophysical experiments on purified recombinant Sgt1 from *Hordeum vulgare* (barley), *Arabidopsis thaliana*, *Saccharomyces cerevisiae* (baker's yeast), and *Homo sapien* (human) that provide the first detailed biochemical characterization of this essential protein. Our study highlights self-association as a property of Sgt1 that is mediated by its TPR domain, but one that exists to varying degrees in different species. We discuss the implications of this self-association in the context of the known functions of Sgt1 in different organisms.

MATERIALS AND METHODS

Design and Cloning of Constructs. Cloning of N-terminal histidine tagged barley Sgt1 (His-HvSgt1, residues 1−373) and *Arabidopsis* Sgt1b (His-AtSgt1b, residues 1−358), one of the two Sgt1 homologues in *Arabidopsis thaliana*, has previously been described (*15*). Histidine-tagged Human Sgt1 (His-HsSgt1, residues 1−333) and yeast Sgt1 (His-ScSgt1, residues 1−395) were generously provided by Dr. Kitagawa and St. Jude Children's Research Hospital, Memphis, TN. Two deletion mutants of barley Sgt1, His-HvSgt1$_{TPR}$ (residues 1−130) and His-HvSgt1$_{\Delta TPR}$ (residues 160−373), were engineered with TEV protease sites and PCR-amplified using the primers 5′-GCGCGGCAGCCATATGGAG-3′ and 5′-GCAGCGGATCCCTATACTGGC-3′ for the His-HvSgt1$_{TPR}$ deletion mutant, and 5′-GGTGAACATATGGAGAATG-CACA-3′ and 5′-GGGATCCTTAATACTCCCACTTC-3′ for the His-HvSgt1$_{\Delta TPR}$ deletion mutant. The PCR products were subcloned into pET15b vector (Novagen, U.K.) to generate constructs with N-termini hexa-histidine sequences.

The sequences of all the constructs were verified by DNA sequencing before transforming into BL21-DE3 (pLysS) (Novagen, U.K.) cell lines for protein expression.

Protein Expression and Purification. Recombinant cells were grown aerobically in LB at 37 °C until mid-log phase. Protein expression was induced with 0.5−1 mM IPTG and growth continued for a further 3 h, after which cells were harvested at 4 °C by centrifugation at 4000 rpm (3501*g*) for 20 min.

To purify the His-tagged proteins, the recombinant cells were resuspended in 20 mM Tris, 0.5 M NaCl, 2 mM TCEP, 2 mM $MgCl_2$, 1 mM PMSF, 0.3 μg/mL DNase, pH 7.5, and lysed by sonication, and the cell debris was removed by centrifugation at 4 °C for 30 min using a speed of 18 000 rpm (38724*g*). The constructs were purified over a nickel-charged resin (Novagen, U.K.) and eluted with an imidazole gradient of 5−750 mM in 20 mM Tris, 0.5 M NaCl, 2 mM TCEP, pH 7.5. To produce cleaved HvSgt1 for specific experiments, the fusion protein was dialyzed against 50 mM Tris-Cl, 150 mM NaCl, 0.5 mM EDTA, 1 mM DTT, pH 8.0, and incubated with 5 U/mg protein of TEV protease (Invitrogen, U.S.A.) at 4 °C for 12 h. All the proteins (His-tagged fusions or the cleaved protein) were further purified by size-exclusion chromatography, dialyzed against the appropriate buffers, and stored at 4 °C for no more than 1 week.

Protein Purity, Mass Spectrometry, and Structure Predictions. The purity of each protein was determined by SDS−PAGE (Figure 1). His-HvSgt1, His-HsSgt1, and HisScSgt1 were susceptible to proteolysis, and these fragments tended to copurify with the full length proteins. We note that the

susceptibility to proteolysis appears to be a characteristic of Sgt1 proteins, since recombinant ScSgt1 purified from insect cells also copurified with a nonspecific cleavage product (*27*). The masses of the proteins were confirmed by denaturing mass spectrometry, using a Qstar tandem electrospray mass spectrometer (ABI Sciex, U.S.A.). Proteins were diluted to 1 μM in 50% acetonitrile and 0.1% formic acid. Recorded masses were His-HvSgt1 44095.9 Da (calculated 44099.2 Da), His-AtSgt1b 42862.9 Da (calculated 42864.6 Da), His-HsSgt1 40175.7 Da (calculated 40150.1 Da), His-ScSgt1 49233.6 Da (calculated 49215.1 Da), His-HvSgt1$_{TPR}$ 17041.89 Da (calculated 17042.8 Da), and His-HvSgt1$_{\Delta TPR}$ 26350.7 Da (calculated 26348.7 Da).

Native-state mass spectrometry was performed on an LCT Premier time-of-flight (TOF) mass spectrometer (Walters Corporation, U.K.) in positive ionization mode. 3 μL of His-HvSgt1 desalted and diluted to a final concentration of 40 μM (1.8 mg/mL) in 50 mM ammonium acetate was introduced via a static nanoflow needle.

Secondary structure predictions were obtained via the Psipred protein structure prediction server http://bioinf.cs.ucl.ac.uk/psipred/psiform.html (*29*), and homology models were generated with the CPH-2.0 server (*30*).

Unless otherwise noted, all the experiments were performed with the His-tag fusion proteins, in buffer with 5 mM DTT or 2 mM TCEP.

Analytical Size Exclusion Chromatography Experiments. Analytical size exclusion chromatography experiments were performed on a Superdex 200 HR 10/30 column (Amersham Biosciences, U.K.) pre-equilibrated with 50 mM Tris-Cl, 5 mM DTT, pH 7.5, and containing 0.2 or 1 M NaCl. The experiments were performed in triplicate at room temperature and using purified proteins from different batches. A sample volume of 100 μL at a flow rate of 0.8 mL/min was used, with protein concentrations of 14−240 μM detected at 280 nm. The relative elution volumes (K_{av}) were calculated from the equation $K_{av} = (V_e - V_o)/(V_t - V_o)$, where V_e is the elution volume of the protein and V_o and V_t are the void and total column volumes, respectively. The K_{av} of proteins with known molecular weights [ferrittin (440 kDa), catalase (232 kDa), aldolase (158 kDa), BSA (66 kDa), ovalbumin (43 kDa), chymotrypsin (25 kDa), and ribonuclease (13.7 kDa)] were plotted against the log of their molecular weights and the apparent molecular weight (Mwt$_{app}$) of the Sgt1 proteins or deletion mutants determined from the plot using the regression equation: $K_{av} = -0.3542$[log of molecular weight] + 2.0889.

Chemical Cross-Linking. Chemical cross-linking reactions were performed with DSS, a water insoluble homobifunctional *N*-hydroxysuccinimide ester, with a spacer arm of 11.4 Å. The cross-linker was prepared in DMSO and added at a final concentration of 0.1 mM to 10 μL of 15 μM of each His-tagged Sgt1 protein or 23 μM of each deletion mutant prepared in 1 X PBS, 5 mM DTT, pH 7.3. After incubating for 15 min at room temperature, the reactions were quenched by adding 50 mM Tris-Cl, pH 7.5. For MALDI-MS analysis of His-HvSgt1$_{TPR}$ the reaction was scaled up to 150 μL. Cross-linked products were resolved by SDS−PAGE and visualized by staining with Coomassie brilliant blue. DSS was purchased from Pierce biotechnology (Rockford, IL).

Analytical Ultracentrifugation. Analytical ultracentrifugation experiments were acquired on a Beckman XL-A analytical ultracentrifuge using an AN 60Ti rotor (Beckman). Sedimentation equilibrium experiments were conducted at rotor speeds of 15791*g* on 4 mg/mL (233.9 μM) His-HvSgt1$_{TPR}$ or at 50355*g* on 4 mg/mL (90.7 μM) His-HvSgt1. Sedimentation velocity experiments were recorded on 0.9 mg/mL (20.4 μM) His-HvSgt1 or 0.9 mg/mL (52.6 μM) His-HvSgt1$_{TPR}$ at 20 °C, using 12 mm path length cells and rotor speeds of 128909*g*. Absorbance scans at 280 nm, taken at 3 min intervals, were recorded for the proteins in 50 mM Tris, 2 mM TCEP, pH 7.5, with 0, 0.2, or 1 M NaCl. Solvent densities and viscosities were computed using SEDNTERP (*31*) and the data analyzed to yield *c*(*s*) distributions with the SEDFIT program of Schuck et al. (*32*).

Circular Dichroism Spectroscopy. CD experiments were acquired on a JASCO 810 spectrophotometer, using a 0.1 cm path length cell maintained at 20 °C. Protein concentration-dependent experiments were performed with 2.8−55.2 μM (0.05 mg/mL to 0.94 mg/mL) of His-HvSgt1$_{TPR}$ in 50 mM Tris-Cl, 10 mM NaCl, 2 mM TCEP, pH 7.5. Urea unfolding studies were conducted with 4, 7.2, 12.2, 20, or 49.7 μM (0.07 mg/mL to 0.85 mg/mL) His-HvSgt1$_{TPR}$ pre-equilibrated for 30 h in 0−4 M urea prepared in the same buffer. To check reversibility of the unfolding process, a sample in 4 M urea was refolded by extensive dialysis against buffer without urea and its CD spectrum recorded and compared with the native protein at a similar concentration. For a comparison of the secondary structures of the reduced and diamide-induced oxidized His-HvSgt1$_{TPR}$ proteins, the CD experiments were performed with 8 μM (0.1 mg/mL) proteins in 50 mM Tris, 50 mM NaCl, pH 7.5, with or without 2 mM TCEP. CD experiments were conducted in triplicate; using samples from three different batches of purified His-tagged proteins. Recorded CD data are the average of the 3 experiments at a particular protein or urea concentration, corrected for contributions from the buffer or urea. Percent helicities were determined with the K2d algorithm, which gives estimates of the percent of protein secondary structure from far UV CD, using a Kohonen neural network (*33*).

Analysis of Urea-Induced Unfolding Curves. The fraction of unfolded protein, F_u, was calculated from the equation

$$F_u = (y_f - y_{obs})/(y_f - y_u) \quad (1)$$

where y_{obs} is the CD signal in molar ellipticity and y_f and y_u are the values for the folded and unfolded conformations. The values for y_f and y_u were obtained by extrapolation of the base lines for the pre- and post-transition regions of the unfolding curves. Data were fit to a two-state unfolding model [D ↔ 2U] in SigmaPlot v9 (Systat software Inc).

Diamide-Induced Oxidation and Native Gel Electrophoresis. Oxidation to preferentially induce the formation of an intramolecular disulfide bond between Cys 84 and Cys 117 was accomplished by treating His-HvSgt1$_{TPR}$ in 50 mM Tris-Cl, 150 mM NaCl, pH 7.5, with 0.1 mM diamide for 15 min. Contaminating intermolecular disulfides were removed by size exclusion chromatography. The purity of the oxidized protein was verified by nonreducing SDS−PAGE. The diamide-induced oxidized His-HvSgt1$_{TPR}$ or oxidized protein that had subsequently been reduced by the addition of 2 mM DTT, at protein concentrations of 5−22 μM (0.09−0.38 mg/mL) were resolved on a 15% native gel using a constant

current of 6 mA and a 25 mM Tris/19.5 mM glycine running buffer. The native gel was prepared according to the method of Laemmli (*34*) without SDS. Resolved proteins were visualized by staining with Coomassie brilliant blue.

In-Gel Digest and Identification of Cross-Linked Products. In-gel digests of bands corresponding to the DSS-cross-linked His-HvSgt1$_{TPR}$ dimer followed protocols described elsewhere (*35*). MALDI-MS to identify cross-linked dimers was performed on an Applied Biosystems 4700 Proteomics Analyzer. Peptides were identified with the GPMAW software (*36*) by comparing the masses of the fragments (mass tolerance 1 Da) with all possible tryptic or cross-linked tryptic digest sequences within His-HvSgt1$_{TPR}$.

RESULTS AND DISCUSSION

Gel-Filtration Chromatography Suggests Sgt1 Reversibly Self-Associates. Preliminary experiments on purified Sgt1 from barley indicated the protein self-associated. We therefore explored this in more detail through concentration-dependent analytical size exclusion chromatography experiments on purified His-tagged Sgt1 from barley, *Arabidopsis*, baker's yeast, and human. Plots of the apparent molecular weights calculated from the elution volumes of the Sgt1 proteins at protein concentrations of 6−184 μM and in 50 mM Tris-Cl, 5 mM DTT, 0.2 M NaCl, pH 7.5, are shown in Figure 2A. His-HvSgt1 eluted at volumes corresponding to apparent molecular weights of 111 kDa to 167 kDa (in relation to globular protein calibrants). Similarly, His-AtSgt1b eluted at volumes corresponding to apparent molecular weights of 100.9 kDa to 115.1 kDa. His-ScSgt1, with a monomeric molecular weight of 49.2 kDa, eluted at volumes corresponding to apparent molecular weights of 152.7 kDa to 204.8 kDa, while His-HsSgt1 eluted with an apparent molecular weight of 56.7−57.2 kDa, slightly larger than the monomeric molecular weight of 40.2 kDa.

The changes in apparent molecular weights of His-HvSgt1, His-AtSgt1b, and His-ScSgt1 as a function of concentration are indications that these proteins form higher order complexes, while the constant value for His-HsSgt1 in this experiment is consistent with the absence of such higher order structure. The elution profile of a protein on a size exclusion chromatography column depends on both the size and shape of the protein. In computing the apparent molecular weights of the Sgt1 proteins, the assumption is that the proteins are globular. For nonglobular proteins, such an assumption can result in significant deviations from their actual molecular weights, which can lead to an overestimation of their oligomeric states. For example, yeast Hsp90 elutes as a high molecular weight complex of 360 kDa, suggestive of a tetramer (*37*), although from all indications, the protein is a dimer. In our case, His-HsSgt1, which does not appear to self-associate, elutes as a 57 kDa protein, which is significantly larger than the monomeric molecular weight of 40.2 kDa. One possible explanation is that the protein is nonglobular and so elutes much earlier than expected. We return to this point below.

To rule out the possibility that the hexa-histidine tag might have contributed to the self-association of the His-tagged proteins, the experiment was repeated with His-HvSgt1 that had previously been digested with TEV protease to remove all additional residues from the expression vector. Since there

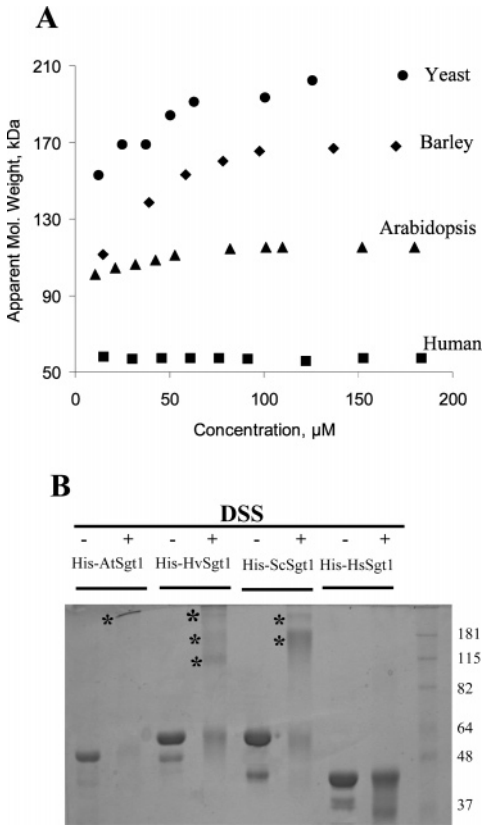

FIGURE 2: Analytical size exclusion chromatography and chemical cross-linking. (A) Plots of apparent molecular weight as a function of protein concentration for His-ScSgt1 (●), His-HvSgt1 (◆), His-AtSgt1b (▲), and His-HsSgt1 (■). Increases in the apparent molecular weights were observed for His-ScSgt1, His-HvSgt1, and His-AtSgt1b but not His-HsSgt1. The experiment was performed in 50 mM Tris-Cl, 0.2 M NaCl, 5 mM DTT, pH 7.5. (B) DSS cross-linking of 15 μM of histidine-tagged Sgt1 proteins in 1X PBS, 5 mM DTT and pH 7.5. Additional bands migrating close to 115 kDa, 181 kDa, or >181 kDa (denoted with asterisks) were observed in the presence of the cross-linker (+) for His-HvSgt1, His-ScSgt1, and His-AtSgt1b, respectively, but not for His-HsSgt1.

was no significant difference between the elution profile of the tagless protein (data not shown) and the His-tagged protein, we conclude that having the histidine tag does not affect the self-association of the protein.

To gain further insight into the self-association of the proteins, DSS cross-linking experiments were performed on the His-tagged proteins. DSS is an NHS-ester cross-linker, which specifically cross-links primary amines within 11.4 Å of each other. The reaction performed with 15 μM Sgt1 proteins and resolved by SDS−PAGE is shown in Figure 2B. In the presence of DSS (+), major bands migrating close to 115 kDa and minor bands migrating >181 kDa were observed for His-HvSgt1. Given that in the absence of DSS (−) the 44.1 kDa His-HvSgt1 protein migrates close to 64 kDa, the major cross-linked band most likely corresponds to the dimer. Bands migrating ≥181 kDa were also observed for the cross-linked 49.2 kDa HisScSgt1 and the 42.7 kDa AtSgt1b. The anomalously slow migration of the proteins on SDS−PAGE is likely due to the high content of charged residues as well as to regions of native disorder in the C-terminal SGS domain (based on predictions using DISOPRED (*38*)). In contrast to the other proteins, the migration of His-HsSgt1 was similar (close to 48 kDa) in the DSS-cross-linked (+) and untreated (-) protein, confir-

mation that this protein does not form higher order complexes. These results further show that Sgt1 from barley, yeast, and *Arabidopsis* self-associates while that from human does not.

The TPR Domain Mediates Self-Association of His-HvSgt1. In order to ascertain whether self-association is mediated by the TPR region of Sgt1 we focused on the protein from barley. We generated two mutants, one where only the TPR domain was expressed (hereafter referred to as His-HvSgt1$_{TPR}$) and the other where the TPR domain was deleted (hereafter referred to as His-HvSgt1$_{\Delta TPR}$). Both constructs were purified as histidine-tagged fusions and used in analytical gel-filtration and chemical cross-linking experiments as described above. His-HvSgt1$_{TPR}$ (at protein concentrations of 20 μM to 238 μM) (Figure 3A) showed an increase in its apparent molecular weight from 32 kDa to 44 kDa in buffer with 0.2 M NaCl. These masses correspond to ~2−2.5-fold increase over the monomeric molecular weight of 17.1 kDa. Masses computed for His-HvSgt1$_{\Delta TPR}$ were between 49.5 kDa and 52 kDa in the protein concentration of 19−240 μM, which is twice the monomeric molecular mass of 26.4 kDa. Similar to the experiment on the full length proteins, the apparent molecular weights were computed based on globular proteins, and so, although the values could be an indication of dimerization, they could also signify the presence of extended conformations.

Chemical cross-linking of the barley Sgt1 deletion mutants shows the presence of an additional band migrating at ~48 kDa for the DSS cross-linked (+) His-HvSgt1$_{TPR}$ (Figure 3B) and the absence of higher molecular weight bands for His-HvSgt1$_{\Delta TPR}$ ((+) Figure 3B).Taken together, the data from the cross-linking and analytical size exclusion chromatography experiments show that residues within the TPR region of His-HvSgt1 contribute to the formation of a higher order complex in barley Sgt1. The results also indicate that the TPR-deleted mutant, His-HvSgt1$_{\Delta TPR}$, is likely an extended protein, as its earlier elution from the size-exclusion column is not a result of self-association.

To determine whether the self-association of barley Sgt1 is ionic strength dependent, we repeated the analytical size exclusion experiments in high ionic strength buffer. Overall, the changes in the apparent molecular weights of the proteins were not as significant as was observed in 0.2 M NaCl. The apparent molecular weight of His-HvSgt1 at protein concentrations of 13−130 μM (0.6−6 mg/mL) increased from 98 kDa to 107 kDa, while His-HvSgt1$_{TPR}$, at protein concentrations of 21−150 μM (0.4−2.6 mg/mL), increased from 26.6 kDa to 27.5 kDa (Figure 3C). We also noticed that, at this high ionic strength, His-HvSgt1$_{TPR}$ was prone to aggregation.

His-HvSgt1 and His-HvSgt1$_{TPR}$ Form Dimers in Solution. Both analytical gel-filtration and chemical cross-linking experiments demonstrate that His-ScSgt1, HisAtSgt1b, His-HvSgt1, and the deletion mutant, His-HvSgt1$_{TPR}$, self-associate in solution. What is not clear from these experiments is the nature of the higher order complexes that these proteins form. Chemical cross-linking experiments although very informative can be misleading because the reaction depends on a number of factors including the accessibility of lysines (for amine specific cross-linkers) at the self-associating interface. Similarly, the apparent molecular weight in analytical size exclusion experiments might not

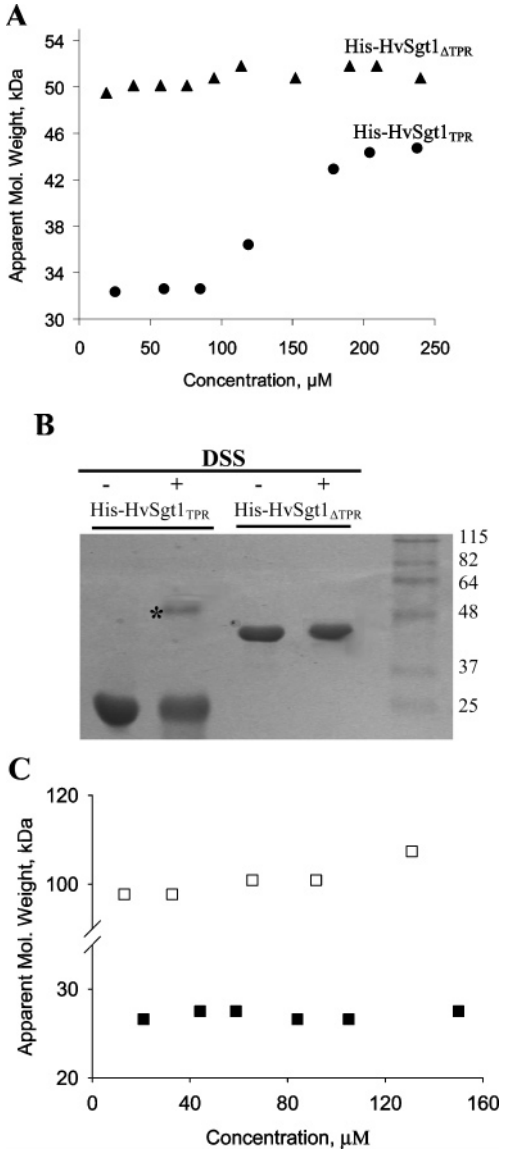

FIGURE 3: Self-association of Barley Sgt1 is mediated by its TPR domain. (A) Plots of apparent molecular weight as a function of protein concentration for His-HvSgt1$_{TPR}$ (●) and His-HvSgt1$_{\Delta TPR}$ (▲). Experiments were performed in 50 mM Tris-Cl, 0.2 M NaCl, 5 mM DTT, pH 7.5, using protein concentrations of 20−240 μM. An increase in apparent molecular weight, indicative of the formation of higher order complexes, was observed for His-HvSgt1$_{TPR}$ but not His-HvSgt1$_{\Delta TPR}$. (B) DSS cross-linking, performed in 1X PBS, 5 mM DTT, pH 7.5, resulted in an additional band (denoted with an asterisk) for His-HvSgt1$_{TPR}$ but not His-HvSgt1$_{\Delta TPR}$. Molecular weight protein markers are shown in the last lane. (C) Plots of the apparent molecular weight as a function of the protein concentration of His-HvSgt1 (□) and His-HvSgt1$_{TPR}$ (■) in 50 mM Tris-Cl, 1 M NaCl, 5 mM DTT, pH 7.5. No significant changes in the apparent molecular weight were observed for either protein at such high ionic strength.

be a true reflection of the oligomeric state of the proteins (reasons previously discussed). To obtain more insight into the type of higher order complexes that is formed, we focused on barley Sgt1 and performed analytical ultracentrifugation (AUC) and native-state nanospray mass spectrometry experiments on the recombinant protein. Results from sedimentation equilibrium experiment of 4 mg/mL (90.7 μM) His-HvSgt1 in 50 mM Tris-Cl, 2 mM TCEP, and 0.01−1M NaCl, pH 7.5, is shown in Table 1. The mass average molecular weight of the protein was ~72 kDa in buffer with

Table 1: Summary of Sedimentation Solution Properties of His-HvSgt1 (44.1 kDa) and His-HvSgt1$_{TPR}$ (17.1 kDa)

construct	ionic strength (M)	$S_{20,w}$[a]	M[b] (kDa)	M[c] (kDa)
His-HvSgt1	0.0−0.01	3.7	70	84
His-HvSgt1	0.2	3.4	57	72
His-HvSgt1	1.0	2.5	33	60
His-HvSgt1$_{TPR}$	0.2	2.6	28	25
oxHis-HvSgt1$_{TPR}$[d]	0.2			17.6

[a] Sedimentation velocity values corrected for buffer densities and viscocities. [b] Molar mass calculated from the sedimentation velocity (cM) analysis. [c] Weight-average molar mass from sedimentation equilibrium analysis. [d] Diamide-induced oxidized barley TPR domain.

0.2 M NaCl and 60 kDa in 1 M NaCl. These values lie between the calculated monomeric molecular weight of 44.1 kDa and the dimeric molecular weight of 88.2 kDa, and are an indication of a subpopulation of monomers and dimers in equilibrium. The slightly reduced apparent molecular weight at the higher ionic strength might be an indication of an increased subpopulation of monomers most likely due to dimer dissociation. At a lower ionic strength (0.01 M NaCl), the apparent molecular weight of 84 kDa was also consistent with the formation of dimers.

Sedimentation velocity data on 0.9 mg/mL (20.4 μM) His-HvSgt1 in different ionic strength buffers is shown in Figure 4A. In low ionic strength buffer, the corrected sedimentation coefficient (s) value was 3.7 s, which corresponds to a calculated molar mass of 70 kDa, somewhat smaller than the calculated mass of 88.2 kDa for a dimer. Increasing the ionic strength to 0.2 M resulted in a decrease in the s-value to 3.4 s with a corresponding molecular mass of ~57 kDa. There is also a noticeable broadening of the sedimentation boundary at this ionic strength, most likely due to heterogeneity in the sample arising from a subpopulation of dimers in equilibrium with monomers. A further increase in the ionic strength to 1 M NaCl results in a decrease in the s-value to 2.5 s and a calculated molecular mass of ~33 kDa. Similar to the sedimentation equilibrium experiments, these calculated molecular weights deviate significantly from those observed at a similar protein concentration in analytical gel-filtration experiments, which we attribute to the extended nature of the Sgt1 protein.

As further confirmation of the AUC results, native-state nanospray mass spectrometry experiments were performed on 40 μM (1.8 mg/mL) His-HvSgt1. The results (shown in Figure 4B) confirm the presence of monomers with a molecular weight of 44.1 kDa and dimers with a molecular weight of 88.4 kDa in solution. These results are in perfect agreement with the expected molecular weights of 44.1 kDa and 88.2 kDa, respectively. Taken together, the analytical ultracentrifugation and mass spectrometry data show clearly that recombinant barley Sgt1 (His-HvSgt1) dimerizes in solution and that the high apparent molecular weight from the analytical gel-filtration experiments is likely a result of an extended conformation of the protein.

To confirm that the protein is indeed nonglobular, we determined its hydrodynamic properties in sedimentation velocity experiments. The frictional and axial ratios of His-HvSgt1 in 1 M NaCl were 1.8 and 10.3, respectively (data not shown), an indication of a highly asymmetric molecule in solution. Other evidence of a noncompact structure are the increased susceptibility to proteolysis (Figure 1) and predicted natively disordered segments within the C-terminal SGS domain. The difference between the molecular weight of the protein determined by sedimentation equilibrium and that determined by size-exclusion chromatography experiments is not unique to Sgt1 but appears to be a characteristic of a number of highly asymmetric proteins that self-associate. An example is the 17 kDa nonglobular antifreeze protein from the winter flounder which forms a dimer in solution, with a molecular weight of 32 kDa, but elutes as an apparent 66 kDa protein on a size-exclusion chromatography column (*39*).

The isolated TPR domain of barley Sgt1, His-HvSgt1$_{TPR}$, also showed the presence of both monomers and dimers in solution in sedimentation velocity and equilibrium analyses (Table 1). In 0.2 M NaCl, the sedimentation coefficient and molecular weight values of 1 mg/mL (58.5 μM) were 2.6 s and 28 kDa, respectively. The weight average molecular weight from sedimentation equilibrium at a similar NaCl concentration was 25 kDa. These values represent a composite average of monomers and dimers in solution. In 1 M NaCl, a component with an s-value of 1.8, calculated molecular weight 15 kDa was observed. Also present at this NaCl concentration was an irreversible aggregate which is an indication that the isolated TPR domain of barley Sgt1 is unstable at high NaCl concentration.

Protein Concentration-Dependent Changes in Structure and Stability. To determine whether the concentration-dependent effect on quaternary structure resulted in a similar effect on the secondary structure, we performed concentration-dependent far UV CD experiments on the isolated TPR domain construct, His-HvSgt1$_{TPR}$, to probe changes in its secondary structure. CD signals at 222 nm, expressed as mean residue molar ellipticities, were normalized such that the signal at the highest protein concentration of 55.2 μM was given a value of 1. A plot of the normalized signals as a function of protein concentration showed concentration-dependence in the range of 2.8 μM to 13.7 μM, while the signals for concentrations >13.7 μM were concentration-independent (Figure 5). To better reflect the dependence of the α-helical content on protein concentration, the CD spectra were deconvoluted to give percent helicities (Figure 5, inset). The data show an increase in the α-helical content from 17% at the lowest concentration of 2.8 μM, to 46% at 7.5 μM and 60% at 13.7−55.2 μM. The results support an increase in helical structure with increasing concentration.

To determine the effect the increase in helical structure might have on the overall stability of the protein, urea-induced unfolding experiments in the protein concentration range of 4−49.7 μM (0.07−0.85 mg/mL) were monitored at 222 nm by far UV CD. The fraction of unfolded protein at each urea concentration was calculated from eq 1. A plot of the fraction unfolded as a function of the urea concentration was fit to a two-state unfolding model, that is folded dimer to unfolded monomer using SigmaPlot v9 (Figure 6). Sigmoidal reversible transitions with midpoints which increased from 1.28 M urea, at a protein concentration of 4 μM, and plateaued at 1.67 M urea, at a protein concentration ≥20 μM, were observed (Figure 6, inset). The shift in transition midpoints is an indication of increased stability of the protein at high protein concentrations and likely reflects the stability of the dimer over the monomer. At all protein concentrations monitored, no detectable intermediates

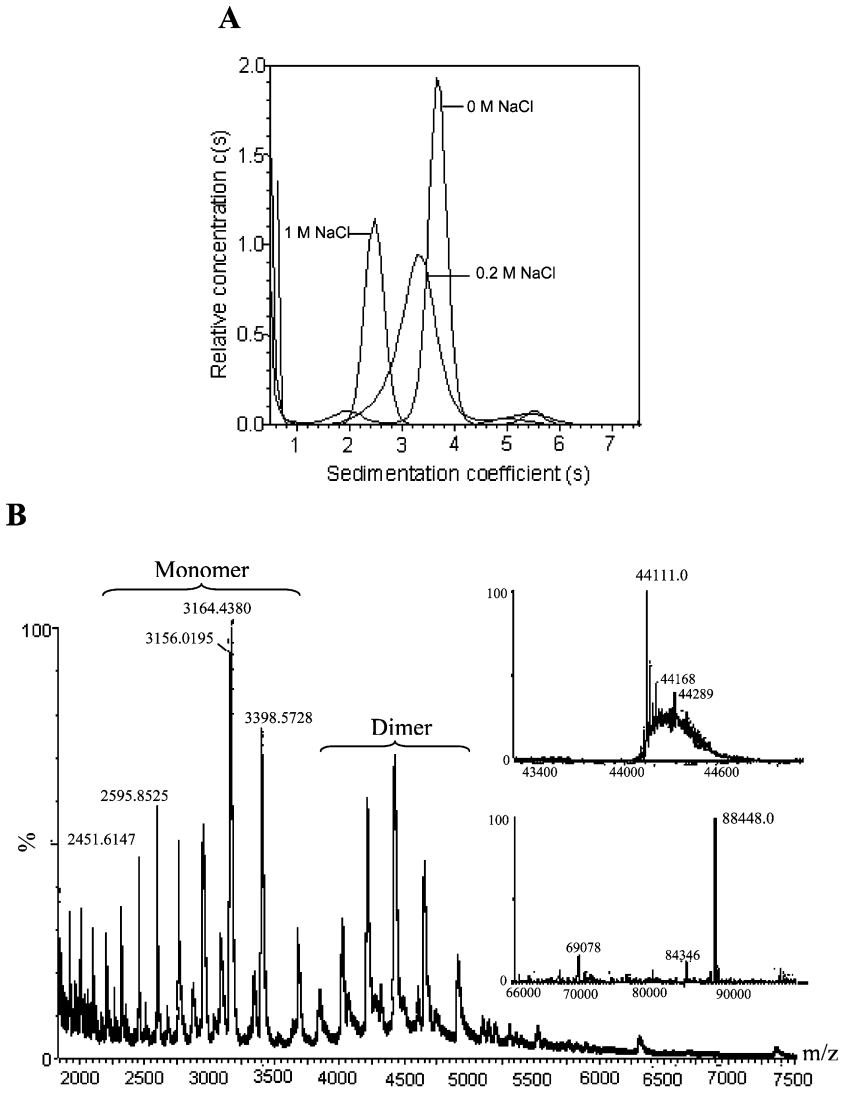

FIGURE 4: His-HvSgt1 forms monomers and dimers in solution. (A). Sedimentation coefficient ($c(s)$) distribution of 0.9 mg/mL His-HvSgt1 in 50 mM Tris, 2 mM TCEP, pH 7.5, with 0, 0.2, or 1 M NaCl. The corrected *s*-values of 3.7 (0 M NaCl), 3.4 (0.2 M NaCl), and 2.5 (1 M NaCl) translate to molecular weights consistent with a dimer−monomer transition. Data were collected at 20 °C. (B) Native-state nanospray mass spectrum of His-HvSgt1 showing the presence of monomers and dimers in solution. The deconvoluted monomer and dimer spectra are shown as insets. Data were acquired on an LCT Premier time-of-flight mass spectrometer (Waters Corporation, U.K.) using 40 μM Sgt1 in 50 mM ammonium acetate.

were observed, implying that dimer dissociation and unfolding are coupled.

An Intramolecular Disulfide Bond within the TPR Region Prevents Self-Association. During the course of this work we noticed that the concentration-dependent ability of Sgt1 to self-associate occurred only under reducing conditions, suggesting a link between disulfide bond formation and the protein's inability to self-associate. There are three cysteines within the primary sequence of barley Sgt1: Cys 84 and Cys 117 within the TPR region and Cys 236 within the CS domain. Since all our data support a TPR-mediated self-association, this rules out any contribution from Cys 236 and so we carried out further investigations using the isolated TPR domain, His-HvSgt1$_{TPR}$. Under oxidizing conditions, there are four possible disulfide bonds that may form: intermolecular disulfide bonds between Cys 84 and Cys 84, Cys 84 and Cys 117, and Cys 117 and Cys 117 and an intramolecular disulfide bond between Cys 84 and Cys 117. We hypothesized that a change in the tertiary packing of the protein due to the formation of the intramolecular disulfide bond and not the intermolecular disulfide bonds was preventing self-association of the protein.

To test this hypothesis, we used low concentrations of diamide to induce the formation of an intramolecular disulfide bond between Cys 84 and Cys 117. To verify that an intramolecular disulfide bond had formed, the diamide-induced oxidized protein (hereafter denoted as oxHis-HvSgt1$_{TPR}$) was subjected to SDS−PAGE under nonreducing conditions. Proteins with an intramolecular disulfide bond usually exhibit a faster electrophoretic migration due to a decrease in chain flexibility and hydrodynamic volume (*40*). This difference in migration allows discrimination between reduced and oxidized proteins. oxHis-HvSgt1$_{TPR}$ exhibited a faster electrophoretic mobility by both native and nonreducing gel electrophoresis. Further evidence for the formation of a disulfide bond was that, on adding excess DTT to the oxidized protein, its electrophoretic migration was similar to the native protein under reducing conditions (data not

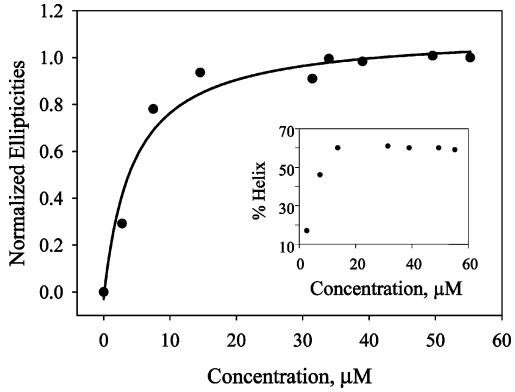

FIGURE 5: Concentration-dependent CD of His-HvSgt1$_{TPR}$. Normalized ellipticities at 222 nm as a function of His-HvSgt1$_{TPR}$ concentrations. The solid line is the best fit to the data. Inset: The α-helical content, as a function of the protein concentration increased from 17 to 60%. The CD experiments were performed at 20 °C using protein concentrations of 2.8−55.2 μM in 50 mM Tris, 10 mM NaCl, 2 mM TCEP and pH 7.5. This plot is an average of three separate experiments.

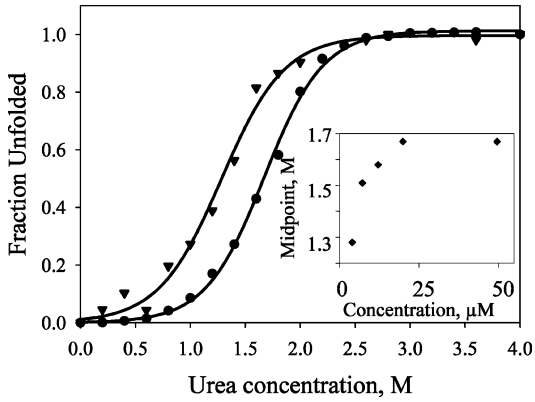

FIGURE 6: Concentration-dependent stability experiments. Urea unfolding curves monitored at 20 °C of His-HvSgt1$_{TPR}$ at 4 μM (▲) or 49.7 μM (●). Curves were generated as explained in Materials and Methods. Sigma Plot v.9 was used to fit the data to a two-step unfolding model (solid line). Inset: Plots of the transition midpoints (1.28, 1.51, 1.58, 1.67, and 1.67) from the urea unfolding experiments as a function of protein concentration (4, 7.2, 12.2, 20, and 49.7 μM). Samples were in 50 mM Tris-Cl, 10 mM NaCl, 2 mM TCEP, pH 7.5, with 0−4 M urea. This plot is an average of two independent experiments.

shown). This, together with an essentially monomeric molecular weight of 17.6 kDa determined from sedimentation equilibrium experiments of the oxidized TPR domain (Table 1), argues for the formation of the intramolecular disulfide bond.

The secondary structure of oxHis-HvSgt1$_{TPR}$ and His-HvSgt1$_{TPR}$ as probed by far UV CD spectroscopy revealed significant differences between the two forms of the protein (Figure 7A). Both proteins exhibited negative ellipticites at 208 and 222 nm, characteristic of proteins with significant α-helical content. Comparison of the ratio of the signals at Θ_{222} and Θ_{208} gave values of 0.92 for oxHis-HvSgt1$_{TPR}$ and 1.22 for His-HvSgt1$_{TPR}$. While the value for oxHis-HvSgt1$_{TPR}$ lies between that commonly observed for a regular helix (∼0.83) and a coiled-coiled structure (≥1), the value for His-HvSgt1$_{TPR}$ indicates that the helical structure present is largely in a coiled-coil conformation (*41*).

Concentration-dependent analytical size exclusion chromatography experiments of oxHis-HvSgt1$_{TPR}$ in buffer with

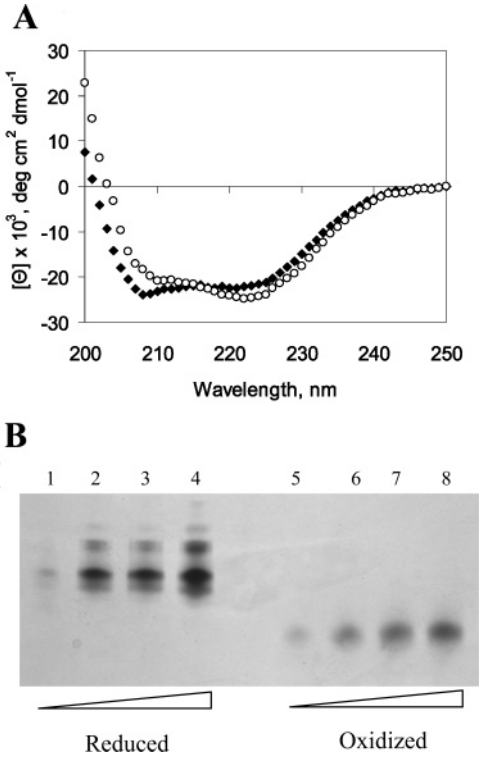

FIGURE 7: CD and native gels of oxidized and reduced barley TPR domain. (A) Overlay of the far UV CD spectra of the oxidized, oxHis-HvSgt1$_{TPR}$ (◆) or reduced, His-HvSgt1$_{TPR}$ (○) forms of the TPR domain of barley Sgt1. A decrease in the signal at 222 nm and an increase in the signal at 208 nm observed for oxHis-HvSgt1$_{TPR}$, compared to His-HvSgt1$_{TPR}$, is an indication of a coiled-coil to helix transition. CD data are the average of 3 scans, acquired at 20 °C using protein concentrations of 8 μM in 50 mM Tris, 50 mM NaCl, pH 7.5, with or without 2 mM TCEP. (B) Native gels of His-HvSgt1$_{TPR}$ (lanes 1−4) or oxHis-HvSgt1$_{TPR}$ (lanes 5−8) at protein concentrations of 5 μM (lanes 1 and 5), 9 μM (lanes 2 and 6), 15 μM (lanes 3 and 7), or 22 μM (lanes 4 and 8). Additional bands indicating the formation of a higher order complex are observed for the reduced but not the oxidized protein.

0.2 M NaCl and at similar protein concentrations used for His-HvSgt1$_{TPR}$ did not show changes in the apparent molecular weight with increasing protein concentrations (data not shown). We also performed native gel electrophoresis on His-HvSgt1$_{TPR}$ and oxHis-HvSgt1$_{TPR}$ in the concentration range of 5−22 μM. Additional bands with increasing protein concentration were observed for the reduced protein, while the single band observed for oxHis-HvSgt1$_{TPR}$ only increased in intensity with a similar increase in protein concentration (Figure 7B). These results show that the formation of an intramolecular disulfide bond significantly affects the ability of the protein to self-associate.

To explain this intriguing result, we combined our biochemical data with a bioinformatic analysis of the TPR domain. Figure 8A is an alignment of the TPR region of barley (HvSgt1), rice (OsSgt1), tobacco (NbSgt1), *Arabidopsis thaliana* (AtSgt1a and AtSgt1b), human (HsSgt1), and baker's yeast (ScSgt1) Sgt1. The two cysteines, Cys 84 and Cys 117, within the TPR region of barley Sgt1 are conserved in the plant Sgt1 proteins. Additionally, Cys117 is conserved between the plant Sgt1 proteins and human Sgt1. Psipred (*29*), a protein secondary structure prediction algorithm, predicts seven helices within the TPR domain of barley Sgt1 (denoted with blue bars in Figure 8A). Based on this

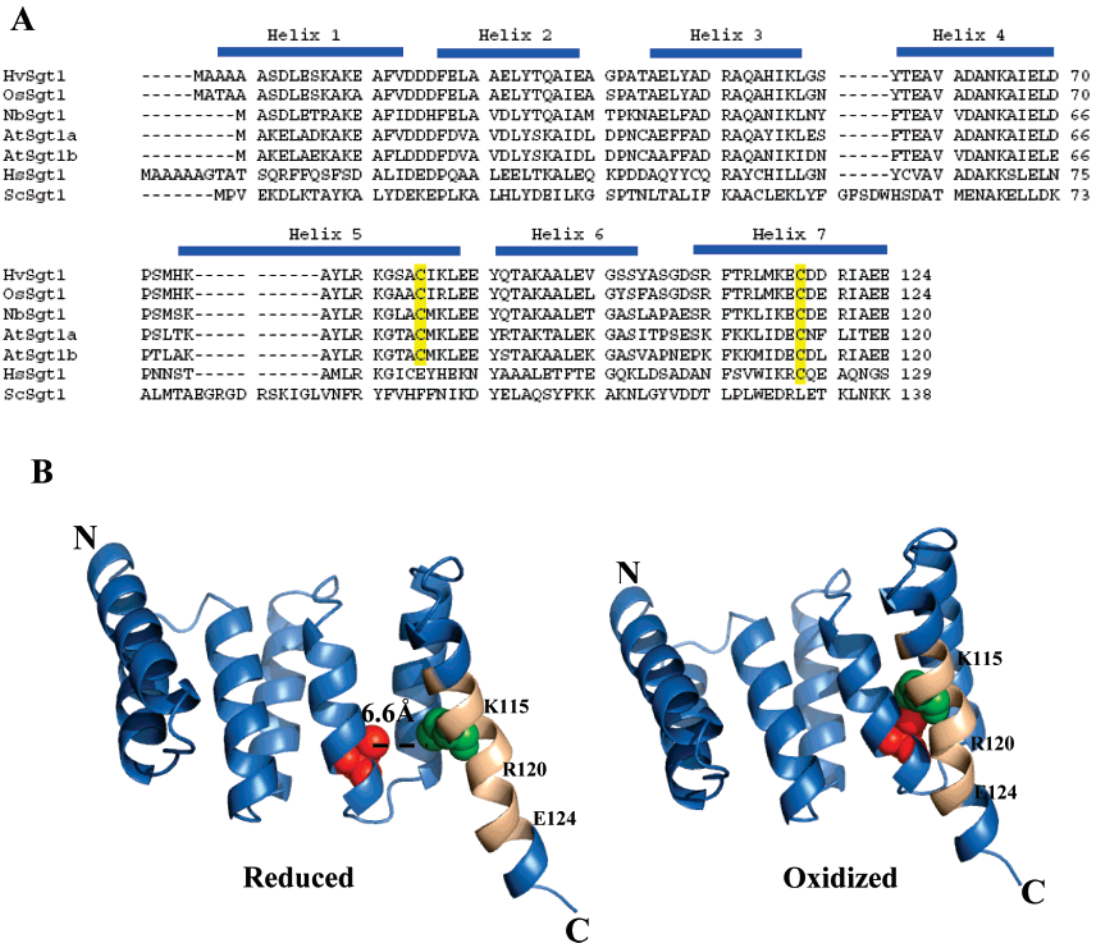

FIGURE 8: Structure predictions of the TPR domain of barley Sgt1. (A) Sequence comparison of the TPR region of HvSgt1 (barley, accession number AF 439974), OsSgt1 (rice, accession number AF 192467), NbSgt1 (tobacco, accession number AF 494083), AtSgt1a and AtSgt1b (*Arabidopsis thaliana*, accession numbers AF 439975 and AF 439976), HsSgt1 (human, accession number AF 132856), and ScSgt1 (baker's yeast, accession number AAB48841). The blue bars represent predicted helical regions (*29*); conserved cysteines are highlighted in yellow. (B) Model of barley Sgt1 (residues 1−130), with space-filling representations of Cys84 (red) and Cys117 (green). The structure was obtained by homology modeling using the crystal structure of the TPR domain of protein phosphatase 5 (*4*) as template. The reduced protein was generated with the CPH models-2.0 server http://www.cbs.dtu.dk/services/CPHmodels/ (*30*). The oxidized protein was generated after energy minimization. Images were produced in PyMOL; http://www.pymol.org (*49*).

prediction, Cys84 and Cys117 are within the fifth and seventh helices, respectively. A model of the TPR domain of barley Sgt1 based on the structure of the TPR domain of protein phosphatase 5 (PDB id 1A17; 30% sequence identity) is shown in Figure 8B with Cys84 (red) and Cys117 (green) shown in space filling representation. In the reduced form (Figure 8B, left), the sulfur−sulfur distance of the two cysteines is 6.6 Å, which is greater than the ideal 2.08 Å required for the formation of a disulfide bond. This implies that for an intramolecular disulfide bond to form, the inter-cysteine distance would need to be shortened, which could occur as a result of a modest conformational rearrangement. This would result in helices 5 and 7 being closer together (Figure 8B, right). The formation of the intramolecular disulfide bond, which prevents self-association, might be a plant-specific mechanism since yeast Sgt1, which also self-associates, and human Sgt1, which does not, both lack these conserved cysteines. Given that the "crystallographic dimer" observed in the monoclinic and tetragonal crystal structures of the TPR domain of cyclophilin 40 involved intermolecular interactions between the C-terminal helix of one molecule and an adjacent molecule (*14*) and that the isolated PP5-TPR domain also forms a crystallographic homodimer through its C-terminal helix (*4*), we speculate that residues within the C-terminal helix are involved in intermolecular interactions and that, in the case of plant Sgt1, a diamide-induced intramolecular disulfide bond orients the helix in a way that prevents these interactions.

Identification of Residues Involved in Intermolecular Interactions. Having established that His-HvSgt1 self-associates through its TPR domain, we used chemical cross-linking, followed by in-gel tryptic digests and mass spectrometry (reviewed in ref *42*) of the deletion mutant, His-HvSgt1$_{TPR}$, to identify the residues involved in the intermolecular interactions. This bottom-up approach has been used to map the intermolecular contact regions of ParR, a homodimeric DNA-binding protein (*43*) and the molecular interface of the homodimer of apolipoprotein A1 (*44*). Proteins subjected to homobifunctional primary-amine-specific cross-linkers may form intermolecular cross-links or have their surface-exposed lysines modified without forming cross-linked products. In using DSS, an intermolecular cross-link is expected to result in an average mass increase of 138.2 Da, while a surface accessible primary amine, which is conjugated to a hydrolyzed cross-linker, is expected to result in a mass increase of 156.2 Da.

As a first step to determine the efficiency of the method, the His-HvSg1$_{TPR}$ was digested in-solution and analyzed by MALDI-MS. 86% of the sequence was assigned. The unassigned region was mapped to the last 18 residues at the C-terminal end of the protein. Pretreating the native protein with 1% SDS prior to the tryptic digest resulted in the assignments of the previously unidentified C-terminal residues (data not shown). This suggests that the C-terminal residues are not easily accessible to the proteolytic enzyme in the native protein.

When His-HvSgt1$_{TPR}$ was treated with DSS, a lysine-specific cross-linker, sequence coverage was 77%. The resulting peptide mixture included unmodified peptides, peptides modified by partially hydrolyzed cross-linker and a single intermolecular cross-link, which corresponded in mass to residues 113−120 (observed mass 2153.0 Da; expected mass 2153.9). Interestingly, this peptide is within the predicted C-terminal helix of the TPR domain (helix 7 in Figure 8), which our diamide-induced oxidation experiments led us to suggest might be involved in intermolecular associations that promote dimerization. Although we cannot rule out the possibility that other residues not observed by mass spectrometry might also be involved in intermolecular interactions, our data clearly show that residues in the vicinity of K115 (the most likely cross-linking site) are involved in intersubunit associations.

A closer look at this region of the protein for plant, yeast, and human Sgt1 shows the presence of hydrophobic as well as charged residues. Specifically, the last five residues of plant and yeast Sgt1 are rich in highly charged (R/K/E) residues while human Sgt1 is not (Figure 8A). Since we have shown that the self-association of barley Sgt1 is ionic-strength dependent, it is possible that these charged residues mediate dimerization of plant and yeast Sgt1 proteins while their absence in human Sgt1 protein prevents self-association.

CONCLUSIONS

The present study is the first biophysical characterization of the essential eukaryotic protein Sgt1. Surprisingly, we find that the protein shows variable self-association behavior *in vitro*. A key observation from these studies is the role of the TPR domain in mediating the self-association. This behavior appears to mimic another Hsp90-binding TPR-containing protein, Sti1, which has recently been reported to undergo a TPR-mediated dimerization in solution (*45*). As with Sti1, it is not clear whether dimerization is a prerequisite for Sgt1 function *in vivo*. However, with recent reports that the TPR domain likely functions as a regulatory domain to control the steady-state levels of *Arabidopsis thaliana* Sgt1 (*46*) and that the TPR domain of PP5 regulates its phosphatase activity (*47*), the TPR-mediated self-association of barley Sgt1 and possibly *Arabidopsis* and yeast Sgt1 might be a mechanism to regulate their functions. The differences in the propensities of the Sgt1 proteins to self-associate further argue for self-association as a mechanism to regulate specific biological functions. For the plant Sgt1 proteins, which have conserved cysteines that can form intramolecular disulfides thereby preventing self-association, we speculate that this may play a role in disease resistance signaling. Following pathogen attack, plants elicit the hypersensitive response, which is an early defense response that leads to localized cell death and prevents the spread of pathogens. Events preceding the localized cell death include a rapid influx of calcium ions, activation of protein kinase pathways, production of reactive oxygen species such as hydrogen peroxide and hydroxyl radicals, nitric oxide and transcription reprogramming (*48*). Although there is as yet no evidence of the oxidized form of plant Sgt1 *in vivo*, we speculate that by forming an intramolecular disulfide bond and maintaining a predominantly monomeric subpopulation, during the "oxidative burst", plant Sgt1 might act as an "oxidative stress sensor" of pathogen attack.

ACKNOWLEDGMENT

We thank Dr. Katsumi Kitagawa and St. Jude Children's Research Hospital, Memphis, TN, for the human and yeast Sgt1 plasmids. We are grateful to Mrs. Berni Strongitharm and Adam Doyle (University of York Technology Facility), Andrew Peters, and Laetitia Cravello (Waters Corporation, U.K.) for mass spectrometry experiments.

REFERENCES

1. D'Andrea, L. D., and Regan, L. (2003) TPR proteins: the versatile helix, *Trends Biochem. Sci. 28*, 655−662.
2. Sikorski, R. S., Boguski, M. S., Goebl, M., and Hieter, P. (1990) A repeating amino acid motif in CDC23 defines a family of proteins and a new relationship among genes required for mitosis and RNA synthesis, *Cell 60*, 307−317.
3. Lamb, J. R., Tugendreich, S., and Hieter, P. (1995) Tetratricopeptide repeat interactions: to TPR or not to TPR?, *Trends Biochem. Sci. 20*, 257−259.
4. Das, A. K., Cohen, P. W., and Barford, D. (1998) The structure of the tetratricopeptide repeats of protein phosphatase 5: implications for TPR-mediated protein-protein interactions, *EMBO J. 17*, 1192−1199.
5. Kersey, P., Bower, L., Morris, L., Horne, A., Petryszak, R., Kanz, C., Kanapin, A., Das, U., Michoud, K., Phan, I., Gattiker, A., Kulikova, T., Faruque, N., Duggan, K., McLaren, P., Reimholz, B., Duret, L., Penel, S., Reuter, I., and Apweiler, R. (2005) Integr8 and Genome Reviews: integrated views of complete genomes and proteomes, *Nucleic Acids Res. 33*, D297−D302.
6. Chen, M. X., McPartlin, A. E., Brown, L., Chen, Y. H., Barker, H. M., and Cohen, P. T. (1994) A novel human protein serine/threonine phosphatase, which possesses four tetratricopeptide repeat motifs and localizes to the nucleus, *EMBO J. 13*, 4278−4290.
7. Ponting, C. C., and Phillips, C. (1996) Rapsyn's knobs and holes: eight tetratrico peptide repeats, *Biochem. J. 314* (Part 3), 1053−1054.
8. Sikorski, R. S., Michaud, W. A., Wootton, J. C., Boguski, M. S., Connelly, C., and Hieter, P. (1991) TPR proteins as essential components of the yeast cell cycle, *Cold Spring Harbor Symp. Quant. Biol. 56*, 663−673.
9. Ollendorff, V., and Donoghue, D. J. (1997) The serine/threonine phosphatase PP5 interacts with CDC16 and CDC27, two tetratricopeptide repeat-containing subunits of the anaphase-promoting complex, *J. Biol. Chem. 272*, 32011−32018.
10. Lamb, J. R., Michaud, W. A., Sikorski, R. S., and Hieter, P. A. (1994) Cdc16p, Cdc23p and Cdc27p form a complex essential for mitosis, *EMBO J. 13*, 4321−4328.
11. Scheufler, C., Brinker, A., Bourenkov, G., Pegoraro, S., Moroder, L., Bartunik, H., Hartl, F. U., and Moarefi, I. (2000) Structure of TPR domain-peptide complexes: critical elements in the assembly of the Hsp70-Hsp90 multichaperone machine, *Cell 101*, 199−210.
12. Cortajarena, A. L., and Regan, L. (2006) Ligand binding by TPR domains, *Protein Sci. 15*, 1193−1198.
13. Cliff, M. J., Williams, M. A., Brooke-Smith, J., Barford, D., and Ladbury, J. E. (2005) Molecular recognition via coupled folding and binding in a TPR domain, *J. Mol. Biol. 346*, 717−732.

14. Taylor, P., Dornan, J., Carrello, A., Minchin, R. F., Ratajczak, T., and Walkinshaw, M. D. (2001) Two structures of cyclophilin 40: folding and fidelity in the TPR domains, *Structure 9*, 431−438.
15. Azevedo, C., Sadanandom, A., Kitagawa, K., Freialdenhoven, A., Shirasu, K., and Schulze-Lefert, P. (2002) The RAR1 interactor SGT1, an essential component of R gene-triggered disease resistance, *Science 295*, 2073−2076.
16. Liu, Y., Schiff, M., Serino, G., Deng, X. W., and Dinesh-Kumar, S. P. (2002) Role of SCF ubiquitin-ligase and the COP9 signalosome in the N gene-mediated resistance response to Tobacco mosaic virus, *Plant Cell 14*, 1483−1496.
17. Feys, B. J., and Parker, J. E. (2000) Interplay of signaling pathways in plant disease resistance, *Trends Genet. 16*, 449−455.
18. Gray, W. M., Muskett, P. R., Chuang, H. W., and Parker, J. E. (2003) Arabidopsis SGT1b is required for SCF(TIR1)-mediated auxin response, *Plant Cell 15*, 1310−1319.
19. Peart, J. R., Lu, R., Sadanandom, A., Malcuit, I., Moffett, P., Brice, D. C., Schauser, L., Jaggard, D. A., Xiao, S., Coleman, M. J., Dow, M., Jones, J. D., Shirasu, K., and Baulcombe, D. C. (2002) Ubiquitin ligase-associated protein SGT1 is required for host and nonhost disease resistance in plants, *Proc. Natl. Acad. Sci. U.S.A. 99*, 10865−10869.
20. Kitagawa, K., Skowyra, D., Elledge, S. J., Harper, J. W., and Hieter, P. (1999) SGT1 encodes an essential component of the yeast kinetochore assembly pathway and a novel subunit of the SCF ubiquitin ligase complex, *Mol. Cell 4*, 21−33.
21. Steensgaard, P., Garre, M., Muradore, I., Transidico, P., Nigg, E. A., Kitagawa, K., Earnshaw, W. C., Faretta, M., and Musacchio, A. (2004) Sgt1 is required for human kinetochore assembly, *EMBO Rep. 5*, 626−631.
22. da Silva, Correia, J., Miranda, Y., Leonard, N., and Ulevitch, R. (2007) SGT1 is essential for Nod1 activation, *Proc. Natl. Acad. Sci. U.S.A. 104*, 6764−6769.
23. Niikura, Y., and Kitagawa, K. (2003) Identification of a novel splice variant: human SGT1B (SUGT1B), *DNA Sequence 14*, 436−441.
24. Tor, M., Gordon, P., Cuzick, A., Eulgem, T., Sinapidou, E., Mert-Turk, F., Can, C., Dangl, J. L., and Holub, E. B. (2002) Arabidopsis SGT1b is required for defense signaling conferred by several downy mildew resistance genes, *Plant Cell 14*, 993−1003.
25. Takahashi, A., Casais, C., Ichimura, K., and Shirasu, K. (2003) HSP90 interacts with RAR1 and SGT1 and is essential for RPS2-mediated disease resistance in Arabidopsis, *Proc. Natl. Acad. Sci. U.S.A. 100*, 11777−11782.
26. Lee, Y. T., Jacob, J., Michowski, W., Nowotny, M., Kuznicki, J., and Chazin, W. J. (2004) Human Sgt1 binds HSP90 through the CHORD-Sgt1 domain and not the tetratricopeptide repeat domain, *J. Biol. Chem. 279*, 16511−16517.
27. Catlett, M. G., and Kaplan, K. B. (2006) Sgt1p Is a Unique Co-chaperone That Acts as a Client Adaptor to Link Hsp90 to Skp1p, *J. Biol. Chem. 281*, 33739−33748.
28. Nowotny, M., Spiechowicz, M., Jastrzebska, B., Filipek, A., Kitagawa, K., and Kuznicki, J. (2003) Calcium-regulated interaction of Sgt1 with S100A6 (calcyclin) and other S100 proteins, *J. Biol. Chem. 278*, 26923−26928.
29. McGuffin, L. J., Bryson, K., and Jones, D. T. (2000) The PSIPRED protein structure prediction server, *Bioinformatics 16*, 404−405.
30. Lund, O., Nielsen, M., Lundegaard, C., and Worning, P. (2002) CPHmodels 2.0: X3M a Computer Program to Extract 3D Models. Abstract at the CASPS conference A102.
31. Laue, T. M., Shah, B. D., Ridgeway, T. M., and Pelletier, S. L. (1992) Computer-aided interpretation of analytical sedimentation data for proteins in *Analytical Ultracentrifugation in Biochemistry and Polymer Science*, The Royal Society of Chemistry, Cambridge.
32. Schuck, P. (2000) Size-distribution analysis of macromolecules by sedimentation velocity ultracentrifugation and lamm equation modeling, *Biophys. J. 78*, 1606−1619.
33. Andrade, M. A., Chacon, P., Merolo, J. J., and Moran, F. (1993) Evaluation of secondary structure of proteins from UV Circular Dichroism using unsupervised learning neural network, *Protein Eng. 6*, 383−390.
34. Laemmli, U. K. (1970) Cleavage of structural proteins during the assembly of the head of bacteriophage T4, *Nature 227*, 680−685.
35. Nyarko, A., Hare, M., Hays, T. S., and Barbar, E. (2004) The intermediate chain of cytoplasmic dynein is partially disordered and gains structure upon binding to light-chain LC8, *Biochemistry 43*, 15595−15603.
36. Peri, S., Steen, H., and Pandey, A. (2001) GPMAW—a software tool for analyzing proteins and peptides, *Trends Biochem. Sci. 26*, 687−689.
37. Jakob, U., Meyer, I., Bugl, H., Andre, S., Bardwell, J. C., and Buchner, J. (1995) Structural organization of prokaryotic and eukaryotic Hsp90. Influence of divalent cations on structure and function, *J. Biol. Chem. 270*, 14412−14419.
38. Ward, J. J., Sodhi, J. S., McGuffin, L. J., Buxton, B. F., and Jones, D. T. (2004) Prediction and functional analysis of native disorder in proteins from the three kingdoms of life, *J. Mol. Biol. 337*, 635−645.
39. Marshall, C. B., Chakrabartty, A., and Davies, P. L. (2005) Hyperactive antifreeze protein from winter flounder is a very long rod-like dimer of alpha-helices, *J. Biol. Chem. 280*, 17920−17929.
40. Kang, J. G., Paget, M. S., Seok, Y. J., Hahn, M. Y., Bae, J. B., Hahn, J. S., Kleanthous, C., Buttner, M. J., and Roe, J. H. (1999) RsrA, an anti-sigma factor regulated by redox change, *EMBO J. 18*, 4292−4298.
41. Lau, S. Y., Taneja, A. K., and Hodges, R. S. (1984) Synthesis of a model protein of defined secondary and quaternary structure. Effect of chain length on the stabilization and formation of two-stranded alpha-helical coiled-coils, *J. Biol. Chem. 259*, 13253−13261.
42. Sinz, A. (2006) Chemical cross-linking and mass spectrometry to map three-dimensional protein structures and protein-protein interactions, *Mass Spectrom. Rev. 25*, 663−682.
43. Bennett, K. L., Kussmann, M., Bjork, P., Godzwon, M., Mikkelsen, M., Sorensen, P., and Roepstorff, P. (2000) Chemical cross-linking with thiol-cleavable reagents combined with differential mass spectrometric peptide mapping—a novel approach to assess intermolecular protein contacts, *Protein Sci. 9*, 1503−1518.
44. Davidson, W. S., and Hilliard, G. M. (2003) The spatial organization of apolipoprotein A-I on the edge of discoidal high density lipoprotein particles: a mass specrometry study, *J. Biol. Chem. 278*, 27199−27207.
45. Flom, G., Behal, R. H., Rosen, L., Cole, D. G., and Johnson, J. L. (2007) Definition of the minimal fragments of Sti1 required for dimerization, interaction with Hsp70 and Hsp90 and in vivo functions, *Biochem. J. 404*, 159−167.
46. Azevedo, C., Betsuyaku, S., Peart, J., Takahashi, A., Noel, L., Sadanandom, A., Casais, C., Parker, J., and Shirasu, K. (2006) Role of SGT1 in resistance protein accumulation in plant immunity, *EMBO J. 25*, 2007−2016.
47. Yang, J., Roe, S. M., Cliff, M. J., Williams, M. A., Ladbury, J. E., Cohen, P. T., and Barford, D. (2005) Molecular basis for TPR domain-mediated regulation of protein phosphatase 5, *EMBO J. 24*, 1−10.
48. Heath, M. C. (2000) Hypersensitive response-related death, *Plant Mol. Biol. 44*, 321−334.
49. DeLano, W. L. (2002), DeLano Scientific, Palo Alto, CA, U.S.A.

BI700735T